High Temperature Corrosion of Materials (2023) 100:65–83
https://doi.org/10.1007/s11085-023-10165-3

ORIGINAL PAPER

# Temperature Range of Heating Rate Dependent Reactions Leading to Spinel Formation on a Ni-Based Superalloy

**M. P. Taylor[1] · D. Calderwood[1] · T. D. Reynolds[1,2] · N. Warnken[1] · P. M. Mignanelli[2] · M. C. Hardy[2] · D. M. Collins[1]**

Received: 17 March 2023 / Revised: 21 April 2023 / Accepted: 26 May 2023 /
Published online: 24 June 2023


## Abstract

Improved oxidation kinetics for a polycrystalline Ni-based superalloy used in turbine disc applications has been shown to be possible by controlling the heating rate of the first thermal exposure to 5 °C $min^{-1}$. The beneficial effect arises from the formation of a protective layer of $NiCr_2O_4$, instead of the more usually formed doped $Cr_2O_3$. This study shows that it was possible to form the $NiCr_2O_4$ at temperatures up to 725 °C, within the operational conditions for this alloy, and that at higher temperatures $Cr_2O_3$ formed. The improvements in alloy performance extended to the internal oxidation processes where reduced depths of degradation were observed. It is demonstrated here that $Al_2O_3$ formation is less thermodynamically stable when the highly protective $NiCr_2O_4$ oxide is present at the alloy surface compared to the doped $Cr_2O_3$. Synchrotron XRD was performed on samples removed during the heating stage and provided evidence of the oxidation sequence occurring, enabling refinement in the thermodynamic calculations and suggesting an additional route to the formation of the $NiCr_2O_4$.

**Keywords** $NiCr_2O_4$ · Spinel · Ni-based superalloy · Oxidation

## Introduction

High temperature oxidation resistance of alloys can be achieved with the formation of a surface layer of $Al_2O_3$, $Cr_2O_3$ or $SiO_2$ [1, 2]. Factors, such as the concentration of the oxidising species in the alloy and other minor alloying elements, have been found to promote the early establishment of a fully protective oxide at the surface of a nickel-based alloy and also to improve adhesion of the oxide scale to the alloy [1–9]. Spinels, of generic composition $MN_2O_4$, where M and N can be any of a number of elements including Ni, Co, Cr, Mn and Al, can also form under operational conditions in conjunction with $Al_2O_3$ and/or $Cr_2O_3$.

Extended author information available on the last page of the article

However, the spinel group of oxides does not usually show the potential to provide a reliable barrier to oxidation [2, 5, 7, 10–15].

Recently, the formation of a continuous and protective $NiCr_2O_4$ spinel layer was shown to form on a nickel-based superalloy used for turbine discs applications for aero-engines [16, 17]. The reaction routes leading to the formation of this particular spinel and the less protective, faster growing oxides observed in the same study, where a duplex oxide layer formed with $NiCo_2O_4$ dominating, were found to be heating rate sensitive. The range of heating rates studied were 2 to ~ 100 °C $min^{-1}$ and Synchrotron Grazing Incidence X-ray Diffraction (SGIXD) was used to identify the oxides formed [17]. Whilst the method was successful in identifying very thin oxides, it was not possible to unambiguously differentiate between compounds with near identical crystal structures, in particular, NiO & CoO and $NiCo_2O_4$ & $Co_3O_4$. It was, however, conclusive that NiO/CoO and spinels composed of Co and Ni formed during the heating stage up to the test temperature of 650 °C, with the formation independent of heating rate. No evidence was found for $Cr_2O_3$ forming during the heating stage, instead this oxide and the $NiCr_2O_4$ spinel formed during the subsequent 100 h isothermal exposure at 650 °C. When the alloy was heated at 5 °C $min^{-1}$ it was postulated that a sufficiently thick and continuous NiO layer had formed across the surface of the alloy which acted as a precursor in the subsequent reaction:

$$4NiO + 2Cr = NiCr_2O_4 + 3Ni \quad (1)$$

It was proposed that the continuous nature of the initial NiO layer in contact with the alloy formed during the heating stage, and Cr from the alloy, led to a reaction given in Eq. (1). The resultant spinel formed a continuous layer across the surface of the alloy. Calculations of the Gibbs free energy of formation for all the possible oxide reactions concluded that, with the presence of the NiO, the $pO_2$ had the greatest influence at the reaction site for the subsequent oxide formation. This showed that the reaction presented in Eq. (1) was thermodynamically similar to $Cr_2O_3$ formation at the same location, i.e. underneath a growing NiO.

In the earlier work some constraints in the spinel formation were identified, e.g. at the lowest heating rate investigated, 2 °C·$min^{-1}$, non-protective oxidation behaviour was observed [17]. This behaviour has also been reported to occur following a heating rate of 5 °C·$min^{-1}$ on a Ni 25Cr alloy [13]. The upper heating rate boundary, between 10 and 40 °C·$min^{-1}$, was not clearly defined in our earlier work and the only test temperature investigated was 650 °C.

In this paper the reproducibility of the formation of the protective $NiCr_2O_4$ layer is demonstrated. The oxidation kinetics presented are based on mass gain values and demonstrate lower oxidation rates for the $NiCr_2O_4$ compared to the more usual $Cr_2O_3$ formed on this alloy [18–21]. The study here is extended to a wider range of temperatures with an upper temperature limit encountered. The improvement in oxidation performance for this alloy extended to the internal oxidation products. Thermodynamic calculations are used to describe the effect observed.

## Experimental Procedures

The composition of the polycrystalline nickel-based superalloy used in this study, RR1000, is given in Table 1, [22].

Coupon specimens measuring $20\times10\times3$ mm$^3$ were supplied in a proprietary heat-treated condition. The surfaces of the specimens were ground, using water as a lubricant, on successively fine SiC paper down to 1200 grit and polished using diamond suspension down to a 1 µm finish, following the protocol used previously [17]. The edges of specimens were also chamfered to reduce stress accumulation associated with oxide growth at sharp angled corners and edges. The specimens were measured, ultrasonically cleaned in ethanol, weighed and stored in a desiccator prior to testing. Batches of 2 to 4 specimens were placed in clean alumina boats and placed in a tube furnace equipped with a programmable controller, at room temperature. The controller was set to heat to 650, 675, 700, 725 or 750 °C at a heating rate of 5 °C·min$^{-1}$. The duration of the heating stages ranged from 125 to 150 min. During heating, the temperature within the hot section was monitored independently using a calibrated N-type thermocouple, ensuring that the required heating rate was achieved. Once the specimens had reached the test temperature the alumina boats were removed from the furnace and cooled in laboratory air. The samples were reweighed and stored in a desiccator.

For the testing performed at 650, 675 and 700 °C the samples for each temperature were divided into batches to assess the reproducibility of the heating rate effect. Open and closed circles represent the two samples in the first batch tested at each temperature, Fig. 1. Different symbols are used to differential the data from each sample tested. No batch-to-batch variations in the oxidation behaviour were found.

For subsequent thermal exposures under atmospheric air conditions, the specimens were placed in alumina boats and inserted into furnaces at temperature, i.e. the specimens experienced rapid heating to the test temperature for this part of the testing programme. Great care was taken to ensure that the furnace temperatures did not exceed the test temperature and each furnace was logged throughout using independent thermocouples. Testing over the temperature range of 650 to 750 °C was conducted with specimens exposed for periods of 100 h. On completion of each time period, the specimens were removed from the furnace and allowed to cool to room temperature followed by weighing and storage in a desiccator. Mass change data were collected every 100 h for times up to 1000 h. Thermal cycling was chosen for the testing procedure to enable the collection of the mass change data for statistical evaluation and was also to assess the durability of the $NiCr_2O_4$ spinel under multiple thermal transients.

**Table 1** Nominal composition of RR1000 [22]

| | Ni | Co | Cr | Al | Ti | Ta | Hf | Zr | Mo | B | C |
|---|---|---|---|---|---|---|---|---|---|---|---|
| Wt% | bal | 18.5 | 15.0 | 3.0 | 3.6 | 2.0 | 0.5 | 0.06 | 5.0 | 0.015 | 0.027 |
| At.% | bal | 16.5 | 18.0 | 6.4 | 4.3 | 0.63 | 0.16 | 0.04 | 3.0 | 0.08 | 0.13 |

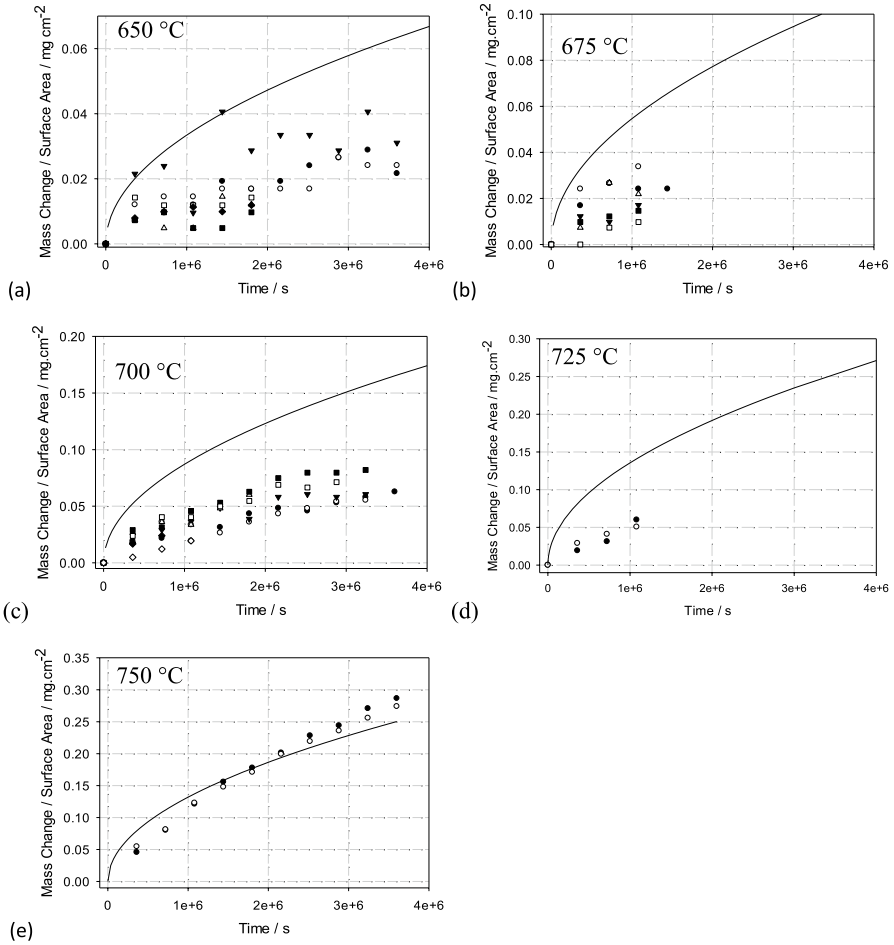


**Fig. 1** Oxidation kinetic data, based on specific mass change, for thermally cycled RR1000 following a heating rate of 5 °C·min$^{-1}$, at **a** 650 °C, **b** 675 °C, **c** 700 °C, **d** 725 °C and **e** 750 °C with the predicted kinetics, (solid lines), for this alloy following a fast heating rate of > 100 °C·min$^{-1}$ [18–20], showing differences in the kinetics linked to the heating rate at temperatures of 725 °C and lower but no difference between the two heating rates at 750 °C. Each sample included in the testing programme has been given a different symbol to enable tracking of changes, all data is included to show the range of the data obtained

To examine the heating stage in more detail, samples of the alloy were prepared to the same surface condition and were placed in individual alumina boats and inserted into a furnace at room temperature and heated up at a rate of 5 °C.min$^{-1}$. A sample was removed when the temperature reached 200, 400, 630 or 800 °C. These samples, representing the oxidation process occurring along the heating stage, were examined in the I11 beam line at the Diamond Light Source using Synchrotron X-ray Diffraction in grazing incidence configuration, SGIXD. The X-ray measurements were acquired with a 15 keV energy (wavelength of 0.8264 Å), which was

calibrated against a NIST 640c Si standard. Each sample was mounted onto the sample stage of the diffractometer using a carbon tab; samples were aligned such that the incident beam was inclined to the sample surface by 1°. Diffraction patterns were acquired over a $2\theta$ scan range 3°–150° using the high-resolution Multi-Analysing Crystals (MAC) detector. The scan time for each sample was 30 min, collected with angular increment of 0.001°. To improve the signal-to-noise ratio the data was re-binned into 0.02° intervals.

Selected specimens were sectioned and prepared for metallurgical examination. These were mounted in cold resin under vacuum. The cross sections were revealed by grinding on SiC papers from 400 to 1200 grit using water as a lubricant. The sections were polished using 6 µm followed by 1 µm diamond suspension in a water-based lubricant and finished on a Si sol. The specimens were ultrasonically cleaned between each stage.

## Results

### Kinetics

Measurements of the specific mass change data against time are shown in Fig. 1, each sample is represented by an individual symbol. At each temperature the open and closed circle symbols give the data for the first two samples at each temperature investigated. As additional batches of samples were prepared these were included in the testing programme and the data recorded using different symbols. This enabled assessing any difference occurring between batches and to track the changes for individual samples. No differences in oxidation behaviour were observed between the batches of samples. Also included, solid line, are the kinetics determined for this alloy under standard oxidising testing procedures with a fast, > 100 °C $min^{-1}$, heating rate to the test temperatures [18–20]. At 650, 675, 700 and 725 °C, Fig. 1a, b, c and d, respectively, the kinetics of the oxide growth for the specimens heated at 5 °C $min^{-1}$ were lower than that determined for the alloy following a fast heating rate. Testing at 750 °C, Fig. 1e, however, revealed no difference in the kinetics obtained for either heating rate. No further testing was conducted at 750 °C.

Parabolic kinetic behaviour is well established for many metals and alloys [23], and is described by:-

$$(\Delta m)^2 = k_p t + C \tag{2}$$

where $(\Delta m)$ is the specific mass change in $mg{\cdot}cm^{-2}$, $t$ is time in seconds, $k_p$ is a parabolic rate constant in $mg{\cdot}cm^{-2}{\cdot}s^{-1}$ and $C$ is a constant which for many purposes is 0 $mg{\cdot}cm^{-2}$.

The means of the mass gain values from all samples at each temperature were calculated and the square of these means were plotted against time, Fig. 2. This shows that the data fits well to parabolic kinetics with the gradient providing the parabolic rate constant for each temperature, Table 2. Also included in Table 2 is the

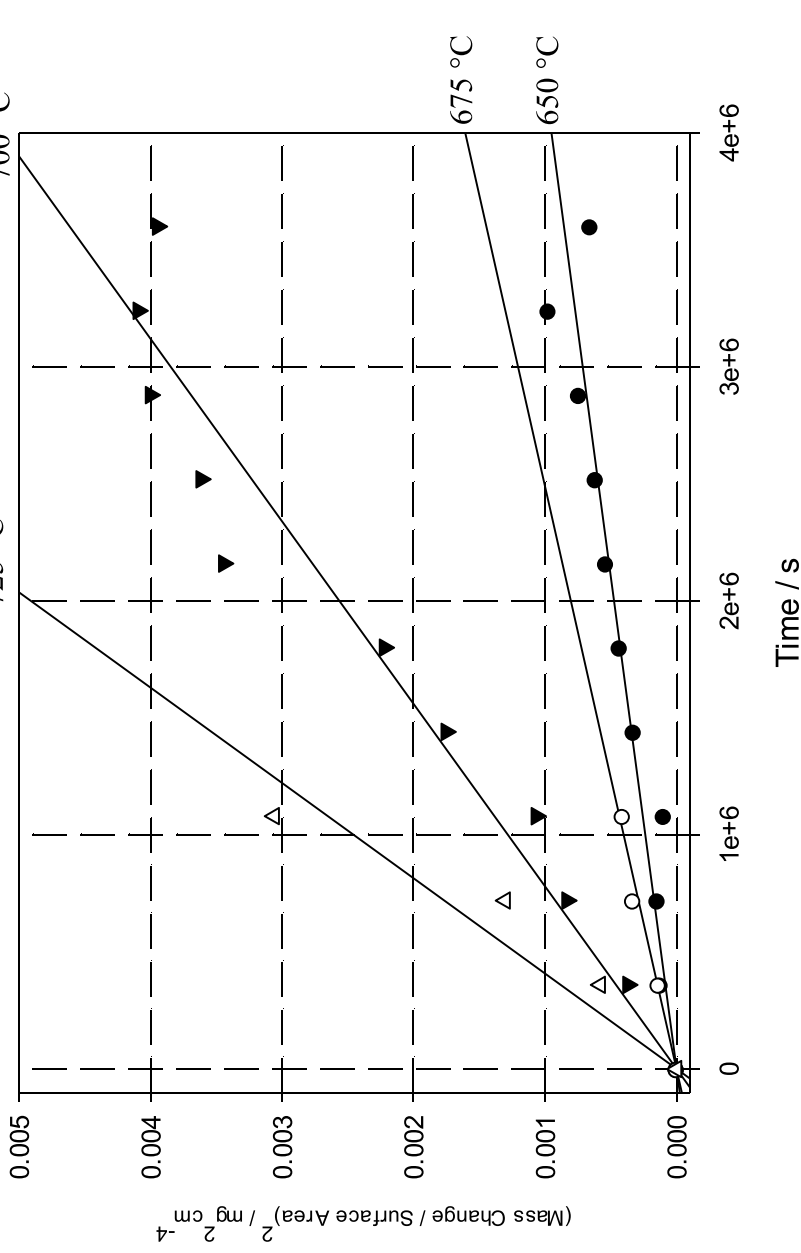


**Fig. 2** Plot of the square of the mean specific mass change at each temperature against time. The gradient of each graph gives the parabolic rate constant at that temperature and are recorded in Table 2

**Table 2** Parabolic growth kinetics at each temperature, note the significant increase in $k_p$ when the temperature increases from 725 to 750 °C

| Temperature/°C | $k_p$/mg$^2$ cm$^{-4}$ s$^{-1}$ |
|---|---|
| 650 | $2.38\times10^{-10}$ |
| 675 | $4.02\times10^{-10}$ |
| 700 | $12.82\times10^{-10}$ |
| 725 | $17.53\times10^{-10}$ |
| 750 | $217.8\times10^{-10}$ |

data obtained at 725 °C. Note the significant increase in the $k_p$ when the temperature changed from 725 to 750 °C.

The data up to and including 725 °C was fitted to the Arrhenius equation:

$$k_p = Ae^{(-Q/RT)} \tag{3}$$

where $k_p$ is a rate constant for the process being studied in mg$^2$ cm$^{-1}$ s$^{-1}$, $A$ is a pre-exponential factor, $Q$ is the activation energy for the oxidation process in J mol$^{-1}$, $R$ is the gas constant of 8.314 J K$^{-1}$ mol$^{-1}$ and $T$ is temperature in K.

The Arrhenius plot shown in Fig. 3 emphasises the step change in the oxidation kinetics from the lower values up to 725 °C and that determined at 750 °C. Also included in Fig. 3 are: lower solid line showing the fit to the data collected in this

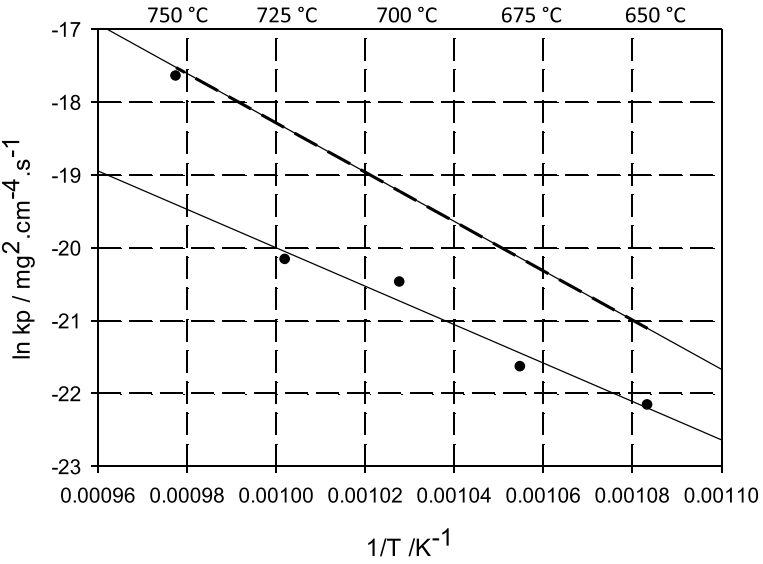


**Fig. 3** Arrhenius plot of the natural log of the parabolic rate constants (points) against 1/$T$ in K$^{-1}$ showing a significant increase when moving from 725 to 750 °C. The activation energy, determined from the gradient of this graph (solid line), gives a value of 205 kJ mol$^{-1}$ for the heating rate of 5 °C·min$^{-1}$ up to and including 725 °C. Also included, dashed line (286 kJ mol$^{-2}$) is the data from previous studies on this alloy using fast heating rates [18, 20] on which the 750 °C data from this study fits

study up to the including 725 °C, and the upper solid line taken from refs [18–20] where a fast heating rate was used.

The gradient for the data plotted, following the 5 °C·min$^{-1}$ heating rate up to 725 °C, gave an activation energy of 205 kJ mol$^{-1}$ for the oxidation reactions, compared to the value of 286 kJ mol$^{-1}$ determined for the alloy following a fast heating rate [18, 20]. This demonstrates the reproducibility of the improvement in the oxidation behaviour of this alloy up to and including 725 °C, which is associated with a heating rate of 5 °C min$^{-1}$ for the initial thermal exposure. Note that all subsequent thermal exposures had a fast, i.e. > 100 °C·min$^{-1}$, heating rate.

The Arrhenius equation describing the oxidation behaviour of this alloy, following a heating rate of 5 °C·min$^{-1}$ is:

$$k_p = 90 \exp^{\left(-\frac{205{,}000}{RT}\right)} \text{mg}^2\ \text{cm}^{-4}\ \text{s}^{-1}. \quad (4)$$

## SGIXD Examination of Samples Removed During Heating Stage

The SGIXD traces of the samples removed at pre-determined temperatures during the initial heating stage, where the heating rate was set as 5 °C·min$^{-1}$, are presented in, Fig. 4. The SGIXD showed no evidence of oxide formation at 200 °C. At 400 °C,

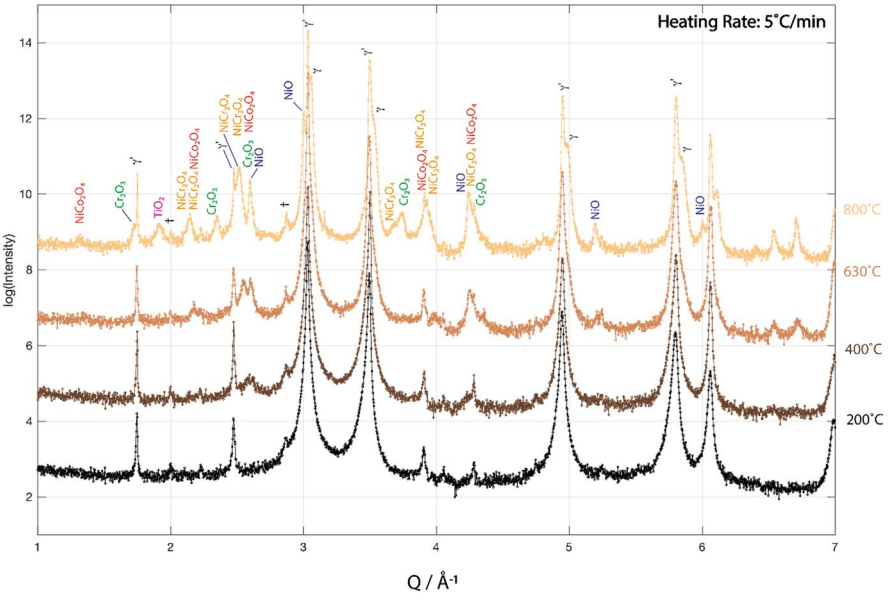


**Fig. 4** SGIXD traces showing the sequence of oxide formation during the heating stage, set to 5 °C min$^{-1}$, showing the peaks from the $\gamma/\gamma'$ phases within the alloy and an unidentified phase labelled '†' also originating from the alloy. The sequence shows the formation of NiO begins at 400 °C, at 630 °C NiO continued to form with evidence of $NiCo_2O_4$, and at 800 °C $NiCr_2O_4$ and $Cr_2O_3$ were present and the peaks associated with $NiCo_2O_4$ diminished

NiO formation was observed. At 630 °C, NiO continued to form, and peaks associated with $NiCo_2O_4$ were also observed. At 800 °C, NiO, $NiCr_2O_4$, $NiCo_2O_4$, $TiO_2$ and $Cr_2O_3$ were present. The peaks associated with NiO oxide formation increased with temperature, however the $NiCo_2O_4$ appeared to diminish at 800 °C, Crystalline $Cr_2O_3$ was only found at 800 °C and not at the lower temperatures, similarly for the $TiO_2$. The latter agrees well with the earlier finding in Ref. [17] where no $Cr_2O_3$ or $TiO_2$ were found to form during that wider heating rate investigation where the test temperature was 650 °C.

## SEM Examination

SEM examination of the surfaces of the specimens showed a clear difference in oxide morphology compared to that formed following a fast heating rate, Fig. 5a and b, respectively. Following a fast heating rate, a surface covering of oxide formed with faster growth at the emergent grain boundaries. With a heating rate of 5 °C $min^{-1}$ the surface of the specimens had a complete covering of oxide with crystallites distributed across the surface, but these were not related to features such as grain boundaries. In addition, no evidence of spallation or cracking of the surface oxide had occurred following the 5 °C $min^{-1}$ heating rate. This lack of spallation or obvious cracking, despite the numerous thermal cycles, demonstrated the durability of the surface oxide.

Cross-sectional examination of the samples revealed that, for temperatures below 750 °C, a thin uniform surface oxide of between 0.3 to 0.7 µm had formed, Fig. 6a. Figure 6b shows the same alloy after 100 h thermal exposure at 700 C following a fast heating rate. Differences are evident in the interface between the external oxides and the alloy and in the amount of internal oxidation products formed. Oxide penetration along grain boundaries was also observed following both heating rates. EDS analysis, of the samples following the of 5 °C·$min^{-1}$ heating rate revealed the surface oxide to be rich in Cr and to contain Ti, Fig. 7. The Ni and Co profiles also showed the presence of these elements within the surface oxide. Due to the resolution limitations, it was not possible to obtain an exact composition at this time, TEM examination will be required to confirm this.

The EDS results showed a depletion profile for Cr into the alloy as a result of the selective oxidation process, but no obvious similar profiles developed for the other elements present. The Al profile showed the formation of a surface layer of $Al_2O_3$ with, again, no obvious depletion of this element from the alloy, as shown in the EDS profile in Fig. 7. Also evident in the cross sections was the formation of $Al_2O_3$ along grain boundaries (g.b.).

The examination of the cross sections through the samples exposed at 750 °C revealed similarities to the findings for this alloy following an initial fast heating rate, Fig. 8. EDS shows that the surface oxide was dominated by Cr and included Ti. The interface between the surface oxide and the alloy was non-planar with light contrast sections of alloy incorporated into the outer oxide scale. The formation of internal $Al_2O_3$ within the sub-surface region of the alloy was also present, as found in earlier studies. The level of internal oxidation was substantially

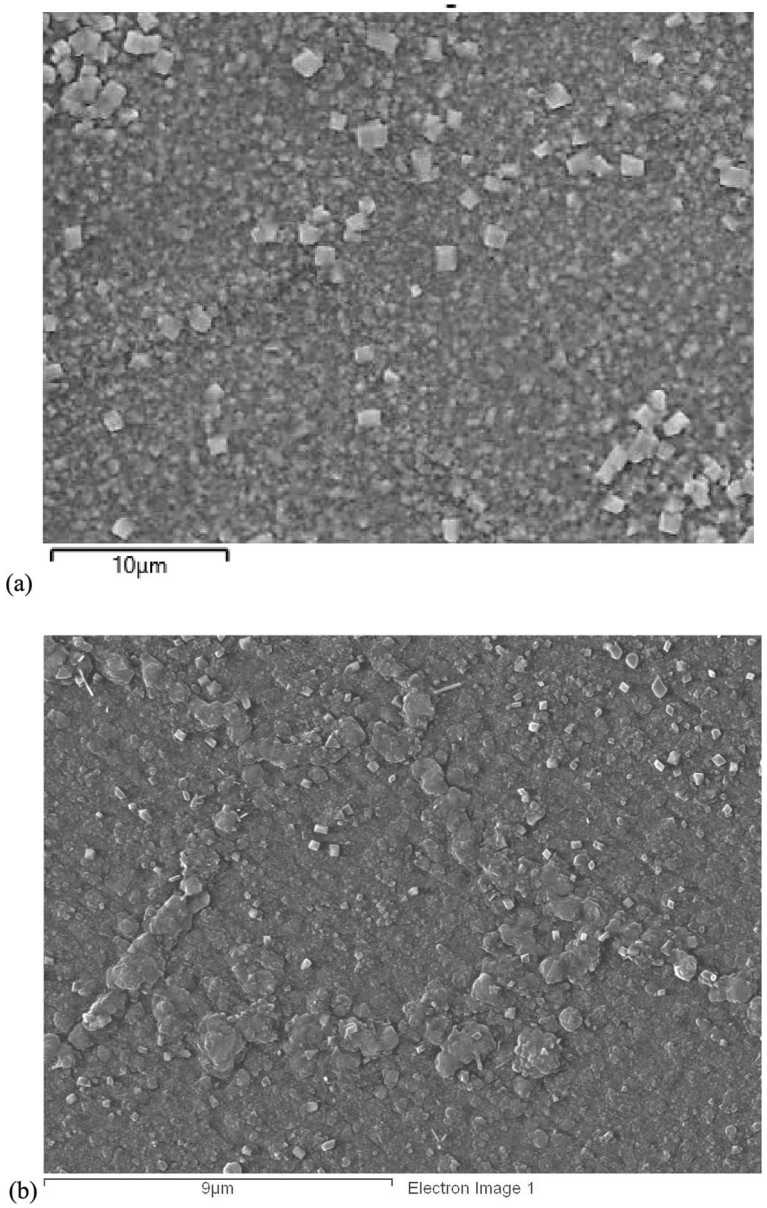


**Fig. 5** SEM images of planar view of **a** a specimen exposed to 700 °C for a total of 1000 h following a heating rate of 5 °C·min$^{-1}$, showing a complete coverage of oxide with larger crystallites, in lighter contrast, distributed across the surface, and **b** a specimen exposed to 700 °C for a total of 100 h following a fast heating rate, showing a complete coverage of oxide with thicker oxide growth at the emergent grain boundaries

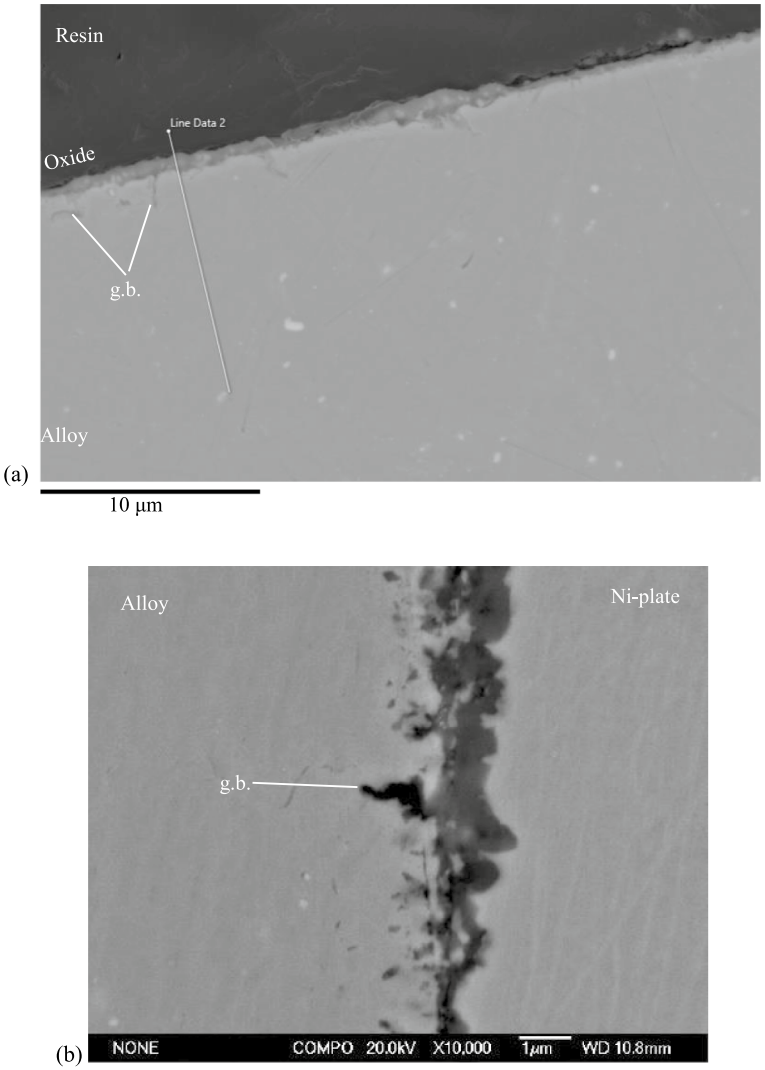


**Fig. 6** SEM images of **a** a section through a sample of RR1000 exposed to a heating rate of 5 °C $min^{-1}$ up to 700 °C, cooled and then exposed to 5 × 100 h thermal exposures at 700 °C showing the formation of a dense relatively uniform surface oxide, some darker contrast oxidation products at grain boundaries (g.b.) and light contrast precipitates within the alloy. The line indicates the site of EDS line scans presented in Fig. 7, and **b** a section through a sample of RR1000 exposed to a fast heating rate up to 700 °C followed by 100 h thermal exposures showing the difference in morphology of the oxidation products

greater than that observed at the lower temperatures. Depletion profiles of Cr, Ti and Al had developed. At test temperatures of 750 °C, following a heating rate of 5 °C·$min^{-1}$, the oxidation behaviour replicated the observations found in earlier studies where all heating rates were fast, i.e. > 100 °C·$min^{-1}$.

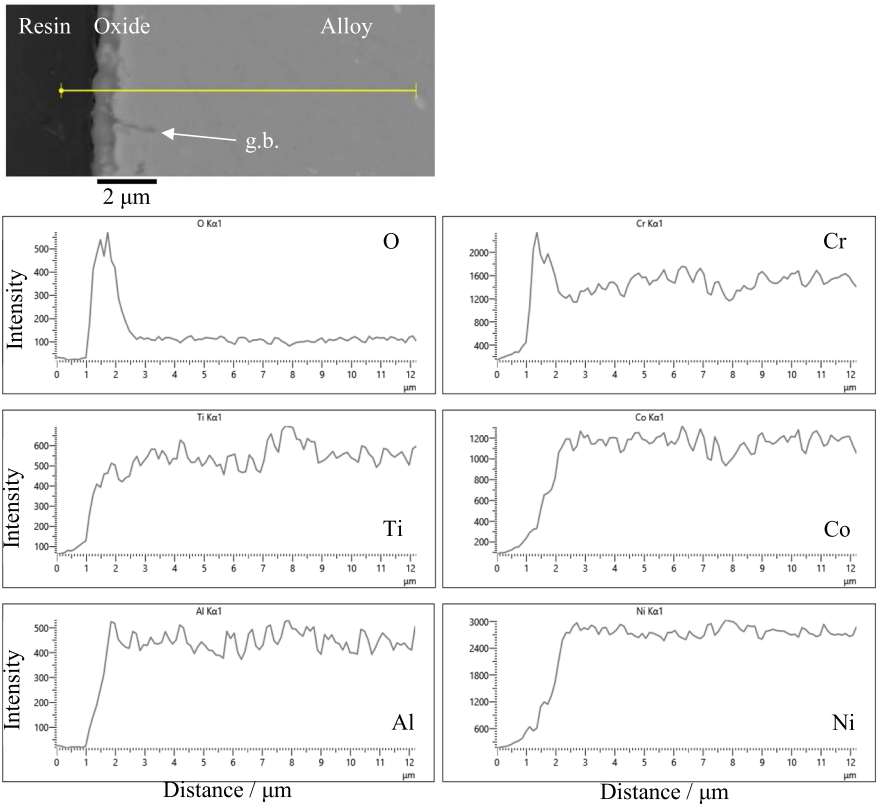


**Fig. 7** SEM image of a section through a sample of RR1000 exposed to a heating rate of 5 °C $min^{-1}$ up to 700 °C, cooled and then exposed to 5 × 100 h thermal exposures at 700 °C with EDS line scans showing the surface oxide dominated by Cr with associated depletion into the alloy. Ti, Ni and Co were also present in the oxide. The profiles show the formation of a layer of $Al_2O_3$ at the surface and along the grain boundaries (g.b.) penetrating into the alloy

## Discussion

The work presented here builds on the findings of an earlier study showing that the chemistry of the surface oxide formed on a Cr-containing Ni-based alloy can be controlled by the rate of heating during the initial thermal exposure up to 650 °C [17]. This was shown to persist for durations up to 4000 h at 650 °C [16]. In the earlier studies it was shown that by controlling the initial heating rate to 5 °C·$min^{-1}$, a surprisingly protective $NiCr_2O_4$ spinel formed. Here it has been demonstrated that this phenomenon was reproducibly obtained and was found to occur for temperatures up to and including 725 °C. The use of 100 h thermal cycles in this study, as opposed to isothermal exposures in Ref. [16], demonstrated the durability of the $NiCr_2O_4$ spinel.

The difference in the oxidation behaviour of the alloy, related to heating rate, was detectable using mass gain measurements up to and including 725 °C, Figs. 1 and 3.

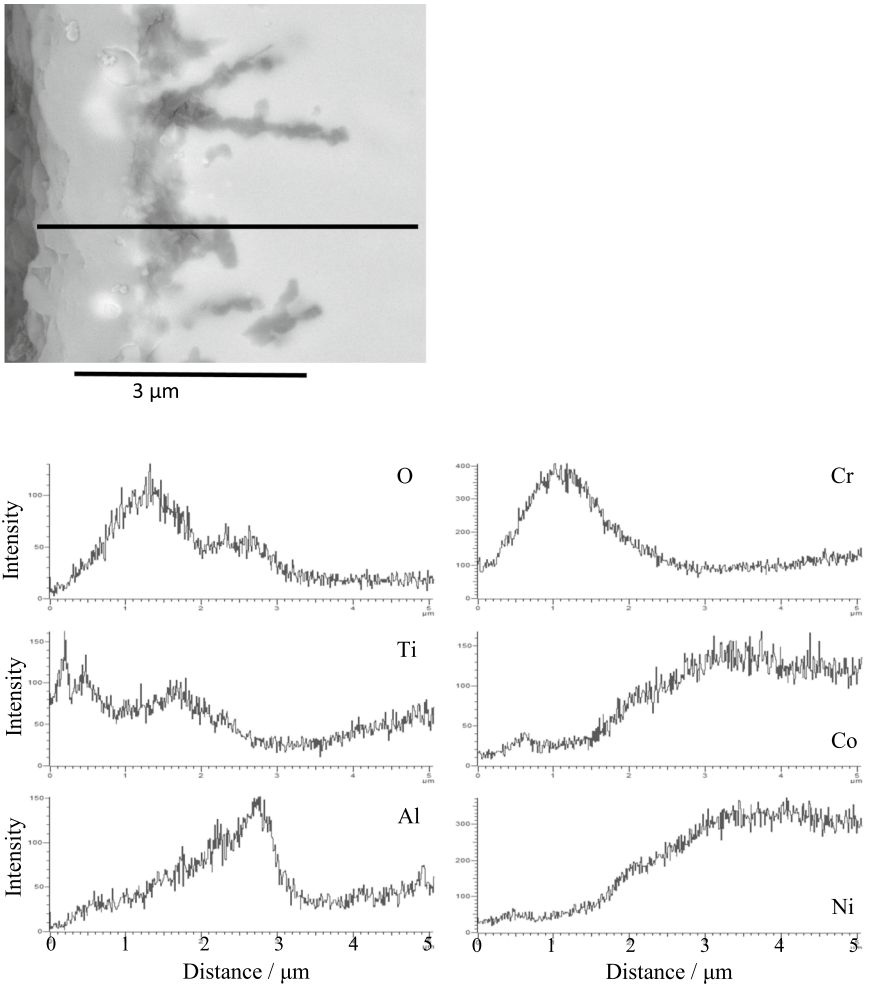


**Fig. 8** SEM image with EDS line scans of a cross section through a specimen heated to 750 °C at 5 °C·min$^{-1}$, followed by 10 × 100 h isothermal exposures at 750 °C showing the more usual oxidation formation for this alloy with a surface chromium-rich oxide with titanium present and aluminium oxide formed internally

Differences in oxide morphology were also evident in SEM examination of planar surfaces, Fig. 6a, when compared to that occurring following a fast heating rates, Fig. 6b. Cross-sectional examination showed the formation of a dense external oxide of uniform thickness and a planar oxide / alloy interface in contrast to the findings at 750 °C which more closely matched the findings following a fast initial heating rate. It was also noted that the amount of internal oxidation occurring in this alloy following a heating rate of 5 °C·min$^{-1}$ was much reduced. This reinforced the evidence from EDS analysis which showed that the chemistry of the oxides formed on this alloy exhibited a sensitivity to the heating rate of the initial thermal transient.

High-resolution SGIXD revealed the oxide formation sequence occurring during the heating stage. This showed that NiO was the first oxide identified, at 400 °C, which continued to grow throughout the heating stage; $(NiCo)_3O_4$ and $NiCr_2O_4$ was observed at 630 °C; with $Cr_2O_3$ and $TiO_2$ only being detected at 800 °C. The sequence of oxide formation, to some extent, confirms the thermodynamic calculations performed in an earlier study [17]. These calculations were made using the Gibbs free energies of formation obtained from Refs. [24, 25] with the temperature-dependent thermodynamic activities for elements within the alloy obtained from the TCNI8 database within Thermo-Calc, [26]. In that interpretation of the oxidation conditions, it was assumed that the faster kinetics of growth of the NiO dominated over the other potential oxides, e.g. $Cr_2O_3$. It was proposed that a heating rate of 5 °C·min$^{-1}$ up to the test temperature of 650 °C, allowed sufficient time for a continuous NiO scale to form across the surface of the specimens. The presence of this NiO scale controlled the $pO_2$ at the alloy—oxide interface and thus influenced all additional oxidation reactions. The $pO_2$, in equilibrium with the formation of NiO was used, where appropriate, in the calculations of the free energy of formation of subsequent reactions. Selected reactions are presented in Fig. 9 and by following the path of the most stable oxide it can be seen that, starting at room temperature and up to approximately 600 K (≈ 350 °C), this oxide would be NiO, as observed in the SGIXD study. At approximately 600 K (≈ 350 °C) the Cr-containing oxides transferred to being the most stable with the predictions showing $Cr_2O_3$ to be more thermodynamically

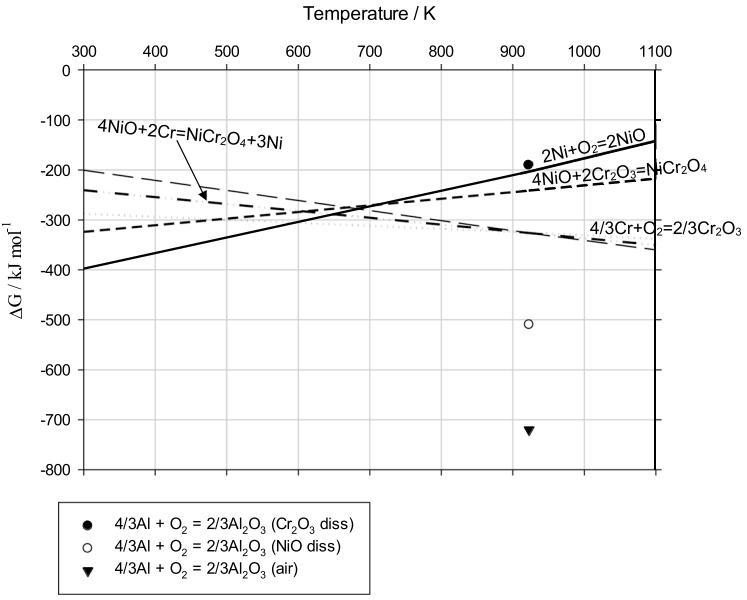


**Fig. 9** Ellingham diagram showing the free energies of formation for a number of relevant oxides formed on the alloy under defined conditions. Also included here are the free energy of formation for $Al_2O_3$ forming in air, under a protective NiO scale (NiO diss) and also under a protective fully stoichiometric $Cr_2O_3$ ($Cr_2O_3$ diss). The activity of Al for these calculations was taken as that in the alloy

stable than $NiCr_2O_4$ up to 900 K (≈ 650 °C). However, the SGIXD results show that $NiCr_2O_4$ formed preferentially to $Cr_2O_3$ over this temperature range and at some point, between 900 and 1100 K (630 and 800 °C), $Cr_2O_3$ became the preferred oxide.

An explanation for the differences between the prediction and the experimental observations can be appreciated by examining the standard thermodynamic equation for the free energy of formation of the oxide $Cr_2O_3$:

$$^4/_3Cr + O_2 = {}^2/_3Cr_2O_3 \tag{5}$$

$$\Delta G = \Delta G^\circ + \ln\left(\frac{a_{Cr_2O_3}^{2/3}}{a_{Cr}^{4/3}a_{O_2}}\right) \tag{6}$$

where $\Delta G^\circ$ is the free energy change for the reaction shown in Eq. 5, $\Delta G^\circ$ is the standard free energy change at a given temperature for pure elements, $a$ is the thermodynamic activity of the component shown.

For simplicity a value for the activity of each oxide was taken as unity in Ref. [17]. However, $Cr_2O_3$ is known to be susceptible to processes such as doping [27–29], which will cause it to depart from full stoichiometry, and thus would be better described by a lower value for the activity of this oxide. By studying Eq. 6 it can be seen that a reduction in the activity of the $Cr_2O_3$ will increase the free energy of formation for this reaction. Thus, the dotted line representing the reaction leading to $Cr_2O_3$ formation in Fig. 9 will shift upwards and changing gradient as indicated by the dashed line. It is proposed here that the results obtained in this study support an increase in the free energy of formation for $C_2O_3$ which places it above that for the $NiCr_2O_4$ reaction (dashed/dotted line) up to somewhere between 900 and 1100 K (630 and 800 °C), and below $NiCr_2O_3$ formation at temperatures of approximately 1100 K (800 °C) and above. It is argued here that the value for the activity of the $NiCr_2O_4$ should remain as unity based on the cross-sectional examination which shows this spinel forms a dense scale and appears to provide greater protection to the more usually formed $Cr_2O_3$ on this alloy, and the SGIXD evidence.

Cross-sectional examination of the samples revealed that the heating rate phenomenon was not only restricted to the composition and morphology of the surface oxide, but there was a noticeable reduction in the amount of internal oxidation of Al Figs. 7 and 8. A thin but detectable layer of Al oxide formed at the interface between the alloy and the Cr-containing continuous surface scale. The Al profile into the alloy was interesting as it did not exhibit the expected depletion associated with the selective oxidation process. One explanation could be that the $Al_2O_3$ is relatively late in forming under these conditions, e.g. as would be the case if the Cr-containing surface oxide was more protective than observed in previous studies and at 750 °C in this study.

To understand the effect on the internal oxidation processes the thermodynamic calculations for $Al_2O_3$ formation, performed in the earlier study, were

revisited. The activity for Al was related to the composition of that element in the alloy [26] and the $pO_2$ was taken as (a) air, (b) in equilibrium with NiO formation, and (c) in equilibrium with a fully stoichiometric $Cr_2O_3$. Plotting these values on the Ellingham Diagram for the temperature of 650 °C, Fig. 9, demonstrates the significant effect of the surface scale protectiveness on the internal oxidation process. It shows that the formation of $Al_2O_3$ can be inhibited underneath a growing, fully stoichiometry, dense surface layer of $Cr_2O_3$, taken here to represent the $NiCr_2O_4$ formed on the surface of this alloy under controlled heating rate conditions. This is supported by the cross-sectional evidence in this study where no significant internal $Al_2O_3$ oxides were present in the alloy following the 5 °C·min$^{-1}$ heating rate up to 725 °C. Under the less protective $Cr_2O_3$ formed at 750 °C, or where fast heating rates are used, internal $Al_2O_3$ formation did occur.

The SGIXD results also showed that $(Ni,Co)_3O_4$ formed at 400 °C but the peak intensity appeared to diminish at higher temperatures, unlike NiO which continued to grow, Fig. 4. One potential explanation for this is the substitution of Cr into the Co sites of the $(Ni,Co)_3O_4$ spinel as this phase continues to grow. With increasing substitution of Cr into the $(Ni,Co)_3O_4$ this spinel will eventually transform to $NiCr_2O_4$ which exhibits a transformation from a cubic to the low temperature tetragonal structure at 46 °C. This is an additional mechanism that may be leading to the formation of $NiCr_2O_4$ on this alloy.

Based on the evidence gathered thus far in this investigation into heating rate sensitivity of the alloy RR1000 a number of potential routes are possible leading to the formation of a protective $NiCr_2O_4$ surface layer. In addition to the mechanism described above, $NiCr_2O_4$ can be formed via the following reactions as previously stated in Ref. [17]:

$$4NiO + 2Cr = NiCr_2O_4 + 3Ni \tag{7}$$

occurring across the majority of the alloy surface, and:

$$NiO + Cr_2O_3 = NiCr_2O_4 \tag{8}$$

at sites where very early formation of $Cr_2O_3$ had occurred, e.g. at emergent grain boundaries. It has been shown that the inclusion of Mo in the alloy will stabilise the $NiCr_2O_4$ [30]. Equation 7 shows that this reaction route leads to the formation of elemental Ni. Once formed this Ni will either oxidise in-situ or diffuse through the oxide. Examination of the micrographs presented in Ref. [30] showed that where the $NiCr_2O_4$ formed, whiskers of NiO were present extending from the outer surface, validating this as a reaction route to the formation of $NiCr_2O_4$.

All the evidence points to an improvement in oxidation resistance for this alloy by controlling the initial heating rate at 5 °C·min$^{-1}$. This approach leads to the formation of a surface scale of $NiCr_2O_4$. The improvement has been found to be restricted to temperatures up to and including 725 °C, which is within the recommended operating conditions for RR1000. The effect of the formation of the more protective externally formed oxide on the alloy was to reduce the amount of internal Al oxidation. A thin layer of $Al_2O_3$ was observed to form at the external oxide—alloy interface which would provide additional oxidation protection. The resultant

protection provided reduced the modifications to the alloy chemistry, as shown in the EDS compositional profiles obtained.

It has also been identified in this study that there is an upper temperature limit to the heating rate sensitivity of this alloy. One possible explanation proposed here is the relative stabilities of the Cr-containing oxides and spinels. Further work is needed to provide a fuller explanation.

## Conclusions

Improved oxidation protection for a nickel-based superalloy, used in disc applications, has been shown to be possible by controlling the initial heating rate to 5 °C $min^{-1}$. The effect was observed up to temperatures of 725 °C. Subsequent heating rates, e.g. due to thermal cycling, did not adversely affect the phenomenon described. In this study the reproducibility of the effect has been demonstrated and refinements to the values for the free energy of formation for the $Cr_2O_3$, to enable prediction of the effect, were proposed. This was supported by data obtained by SGIXD from samples removed at various temperatures during the heating stage, set at 5 °C·$min^{-1}$.

The improvement in oxidation performance of the alloy was detectable using mass change measurements and in cross-sectional examination where a reduction in the amount of internal $Al_2O_3$ formation was found. Thermodynamic predictions demonstrated that there was a significant reduction in the stability of the formation of $Al_2O_3$ in this alloy with the presence of a protective surface scale. The evidence suggested that the improvement in protectiveness of the $NiCr_2O_4$ resulted in the formation of a layer of $Al_2O_3$ at the interface between the alloy and the surface oxide and at grain boundaries, with little intragranular formation. The effect on Al oxidation was observable in the elemental profiles in the alloy underneath the protective $NiCr_2O_4$ compared to that under the $Cr_2O_3$ formed at 750 °C following 5 °C $min^{-1}$. The data obtained from the samples exposed at 750 °C closely matched the findings for this alloy following a fast heating rate.

**Acknowledgements** This work was funded by the Rolls-Royce/EPSRC Strategic Partnership under EP/H022309/1. This work was carried out with the support of the Centre of Electron Microscopy Centre at the University of Birmingham and the Diamond Light Source, instrument I11, proposal number CY28594-2. Dr. Steven Street is thanked for the exploring the possibilities of using synchrotron XRD to investigate surface oxides. Connor Hughes and James Ball, both Ph.D. students at the University of Birmingham, assisted at the Diamond Light Source. The authors acknowledge the guidance of Profs. Arthur Heuer, John Nichols and Hugh Evans on the initial findings of this phenomenon.

**Author Contributions** Conceptualization was contributed by MT; material preparation, data collection and analysis were contributed by MT and DC; formal analysis and investigation were contributed by MT, TR and NW; writing—original draft preparation, was contributed by MT and DC; all authors contributed to writing—review and editing; resources were contributed by PM and MH.

### Declarations

**Conflict of interest** The authors declare there is no conflict of interest.

## References

1. F. H. Stott, G. C. Wood, and J. Stringer, *Oxidation of Metals* **44**, 113 (1995).
2. G. C. Wood and B. Chattopadhyay, *Oxidation of Metals* **10**, 471 (1970).
3. C. S. Giggins and F. S. Pettit, *Journal of the Electrochemical Society* **118**, 1782 (1971). https://doi.org/10.1149/1.2407837.
4. D. P. Whittle and J. S. Stringer, *Philosophical Transactions of the Royal Society A* **295**, 309 (1980).
5. J. S. Stringer, *Oxidation of Metals* **5**, 49 (1972).
6. B. G. Abderrazik, G. Moulin, and A. M. Huntz, *Oxidation of Metals* **33**, 191 (1990).
7. S. C. Tsai, A. M. Huntz, and C. Dolin, *Materials Science and Engineering: A* **212**, 6 (1996).
8. E. A. Polman, T. Fransent, and P. J. Gellings, *Journal of Physics: Condensed Matter* **1**, 4497 (1989).
9. P. Y. Hou and J. Stringer, *Materials Science and Engineering: A* **202**, 1 (1995).
10. C. Greskovich, *Journal of the American Ceramic Society* **53**, 498 (1970).
11. G. Y. Liang, C. Zhu, X. Y. Wu, and Y. Wu, *Applied Surface Science* **257**, 6468 (2011).
12. G. C. Wood and T. Hodgkiess, *Nature* **211**, 1358 (1966).
13. G. Calvarin, R. Moulins, and A. M. Huntz, *Oxidation of Metals* **53**, 25 (2000).
14. B. Chattopadhyay and G. C. Wood, *Oxidation of Metals* **2**, 373 (1970).
15. B. H. Kear, F. S. Pettit, D. E. Fornwalt, and L. P. Lemaire, *Oxidation of Metals* **3**, 557 (1971).
16. T. D. Reynolds, M. P. Taylor, D. J. Child, and H. E. Evans, *Materials at High Temperatures* **35**, 130 (2018).
17. T. D. Reynolds, D. M. Collins, N. K. Soor, S. R. Street, N. Warnken, P. M. Mignanelli, M. C. Hardy, H. E. Evans, and M. P. Taylor, *Acta Materialia* **181**, 570 (2019).
18. M. P. Taylor, H. E. Evans, S. Stekovic, and M. C. Hardy, *Materials at High Temperatures* **29**, 145 (2012).
19. S. Cruchley, H. E. Evans, M. P. Taylor, M. C. Hardy, and S. Stekovic, *Corrosion Science* **75**, 58 (2013).
20. S. Cruchley, M. P. Taylor, R. Ding, H. E. Evans, D. J. Childs, and M. C. Hardy, *Corrosion Science* **100**, 242 (2015).
21. S. Cruchley, M. P. Taylor, H. E. Evans, M. C. Hardy, and D. J. Childs, *Materials Science and Technology* **30**, 1884 (2014).
22. S. J. Hessel, W. Voice, A. W. James, S. A. Blackham, C. J. Small, and M. R. Winstone, Nickel Alloy for Turbine Engine Component. Patent no. EP 0803585 A1. [Online]. Available at: https://www.google.com/patents/EP0803585A1?cl=en (1997).
23. G. Tammann, *Journal of Inorganic and General Chemistry* **111**, 78 (1920).
24. B. O. Knacke, *Thermochemical Properties of Inorganic Substances*, 1st edn. (Springer, Berlin, 1973).
25. D. J. Young, *High Temperature Oxidation and Corrosion of Metals*, 2nd edn. (Elsevier, Amsterdam, 2016).
26. J. O. Andersson, T. Helander, L. Höglund, P. Shi, and B. Sundman, *Calphad* **26**, 273 (2002).
27. A. Holt and P. Kofstad, *Solid State Ionics* **117**, 21 (1999).
28. A. Atkinson, M. R. Levy, S. Roche, and R. A. Rudkin, *Solid State Ionics* **177**, 1767 (2006).
29. A. N. Blacklocks, A. Atkinson, R. J. Packer, S. L. P. Savin, and A. V. Chadwick, *Solid State Ionics* **177**, 2939 (2006).
30. X.-X. Yu, A. Gulec, C. M. Andolina, E. J. Zeitchick, K. Gusieva, J. C. Yang, J. R. Scully, J. H. Perepezko, and L. D. Marks, *Corrosion* **74**, 939 (2018).

## Authors and Affiliations

**M. P. Taylor[1] · D. Calderwood[1] · T. D. Reynolds[1,2] · N. Warnken[1] · P. M. Mignanelli[2] · M. C. Hardy[2] · D. M. Collins[1]**

✉ M. P. Taylor
M.P.Taylor@bham.ac.uk

D. Calderwood
DXC584@student.bham.ac.uk

T. D. Reynolds
Thomas.Reynolds@Rolls-Royce.com

N. Warnken
N.Warnken@bham.ac.uk

P. M. Mignanelli
Paul.Mignanelli@Rolls-Royce.com

M. C. Hardy
Mark.Hardy@Rolls-Royce.com

D. M. Collins
D.M.Collins@bham.ac.uk

[1] School of Metallurgy and Materials, The University of Birmingham, Birmingham B15 2TT, UK

[2] Rolls-Royce, PO Box 31, Derby DE24 8BJ, UK